


[View Journal Online](#)  
[View Article Online](#)

# Regiospecific substitution of the $\beta$ -vinylic $sp^2$ carbon of cyclohexenones bearing the $\alpha$ -chloro- and $\beta$ -tosylate-groups: Single crystal XRD/Hirshfeld surface/*in-silico* studies of three representative compounds

 Arkalgud Satyanarayana Jeevan Chakravarthy <sup>1,2</sup> and Suresh Hari Prasad <sup>2,\*</sup>
<sup>1</sup> Department of Studies in Chemistry, Jnana Bharathi Campus, Bangalore University, Bengaluru, 560056, India  
[jeechakravarthy@gmail.com](mailto:jeechakravarthy@gmail.com) (A.S.J.C.)

<sup>2</sup> Department of Studies in Chemistry, Central College Campus, Bengaluru City University, Bengaluru, 560001, Karnataka, India  
[hariprasad@bub.ernet.in](mailto:hariprasad@bub.ernet.in) (S.H.P.)

 \* Corresponding author at: Department of Studies in Chemistry, Central College Campus, Bengaluru City University, Bengaluru, 560001, Karnataka, India.  
 e-mail: [hariprasad@bub.ernet.in](mailto:hariprasad@bub.ernet.in) (S.H. Prasad).

## RESEARCH ARTICLE



doi 10.5155/eurjchem.11.4.261-275.2020

 Received: 11 August 2020  
 Received in revised form: 14 September 2020  
 Accepted: 15 September 2020  
 Published online: 31 December 2020  
 Printed: 31 December 2020

## KEYWORDS

 Vinyl-chloride  
 Single crystal XRD  
 Molecular docking  
 Competing coupling sites  
 Hirshfeld surface analysis  
 Cyclic  $\alpha,\beta$ -unsaturated ketones

## ABSTRACT

2-Chloro-3-tosyl-5,5-dimethyl-2-cyclohexenone was subjected to a series of regiospecific Suzuki-Miyaura cross-coupling reactions in suspensions of nine different substituted boronic acids, Pd(OAc)<sub>2</sub>, P(Ph)<sub>3</sub>, K<sub>3</sub>PO<sub>4</sub> and 1,4-dioxane solvent, under sealed tube conditions. The regiospecific substitution of the tosyl-group by the aryl group in preference over the chloride- group was observed. A comparison between the bromo- and tosylate group's reactivities is highlighted. Using the methodology, the products: 2-chloro-3-aryl-5,5-dimethyl-2-cyclohexenones were isolated in greater than 85% yields. Good quality crystals of three representative compounds were obtained by slow evaporation technique and subjected to single crystal XRD studies, Hirshfeld surface analysis, 3-D energy framework, and molecular docking studies. Crystal data for compound 3; C<sub>15</sub>H<sub>17</sub>ClO<sub>4</sub>S: monoclinic, space group *P*2<sub>1</sub>/*c* (no. 14), *a* = 8.8687(3) Å, *b* = 10.5537(4) Å, *c* = 16.6862(7) Å,  $\beta$  = 89.807(3)°, *V* = 1561.78(10) Å<sup>3</sup>, *Z* = 4, *T* = 290 K,  $\mu$ (MoK $\alpha$ ) = 0.390 mm<sup>-1</sup>, *D*<sub>calc</sub> = 1.398 g/cm<sup>3</sup>, 13623 reflections measured (6.716° ≤ 2 $\theta$  ≤ 54.962°), 3570 unique (*R*<sub>int</sub> = 0.0467, *R*<sub>sigma</sub> = 0.0512) which were used in all calculations. The final *R*<sub>1</sub> was 0.0452 (*I* > 2 $\sigma$ (*I*)) and *wR*<sub>2</sub> was 0.1019 (all data). Crystal data for compound 5e; C<sub>20</sub>H<sub>18</sub>O<sub>2</sub>FCl: monoclinic, space group *P*2<sub>1</sub>/*c* (no. 14), *a* = 6.4900(5) Å, *b* = 18.6070(13) Å, *c* = 14.2146(11) Å,  $\beta$  = 102.324(2)°, *V* = 1677.0(2) Å<sup>3</sup>, *Z* = 4, *T* = 296(2) K,  $\mu$ (MoK $\alpha$ ) = 0.239 mm<sup>-1</sup>, *D*<sub>calc</sub> = 1.309 g/cm<sup>3</sup>, 25575 reflections measured (6.262° ≤ 2 $\theta$  ≤ 52.224°), 3283 unique (*R*<sub>int</sub> = 0.0494, *R*<sub>sigma</sub> = 0.0307) which were used in all calculations. The final *R*<sub>1</sub> was 0.0875 (*I* > 2 $\sigma$ (*I*)) and *wR*<sub>2</sub> was 0.2056 (all data). Crystal data for compound 5h; C<sub>12</sub>H<sub>13</sub>OSCl: triclinic, space group *P*-1 (no. 2), *a* = 6.7517(6) Å, *b* = 8.8376(9) Å, *c* = 12.6049(12) Å,  $\alpha$  = 109.538(3)°,  $\beta$  = 98.597(3)°,  $\gamma$  = 90.417(3)°, *V* = 699.52(12) Å<sup>3</sup>, *Z* = 2, *T* = 290 K,  $\mu$ (MoK $\alpha$ ) = 0.410 mm<sup>-1</sup>, *D*<sub>calc</sub> = 1.376 g/cm<sup>3</sup>, 28754 reflections measured (6.114° ≤ 2 $\theta$  ≤ 59.288°), 3898 unique (*R*<sub>int</sub> = 0.0544, *R*<sub>sigma</sub> = 0.0349) which were used in all calculations. The final *R*<sub>1</sub> was 0.1101 (*I* > 2 $\sigma$ (*I*)) and *wR*<sub>2</sub> was 0.2481 (all data).

 Cite this: *Eur. J. Chem.* 2020, 11(4), 261-275

 Journal website: [www.eurjchem.com](http://www.eurjchem.com)

## 1. Introduction

In recent years, the pseudohalides (Organomesylates, nonaflates, tosylates, and triflates) have proved as useful substitutes thereby replacing organic halides in cross-coupling reactions [1,2]. There exists interest among scientists worldwide to study the regiospecific control over multiple competing coupling sites [3]. In particular, organotosylates are emerging as new coupling partners in the Suzuki-Miyaura cross-coupling reactions. They form suitable economical pseudohalide alternatives to halides, due to their high stability and easy handling.

Literature reports are available for the coupling of aryl-/alkyl-tosylates with aryl boronic acid [4]. However, no reports exist for the regiospecific substitution of the cyclic vinylic

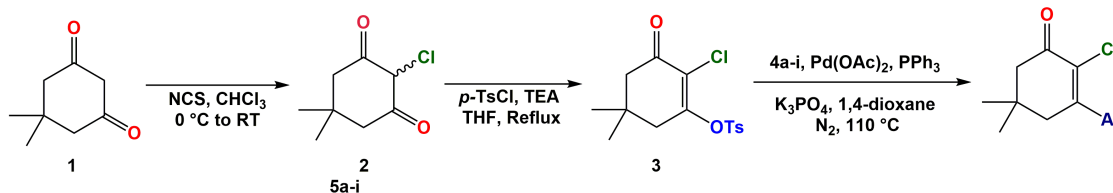
tosylate group preferentially over the vinylic chloride, in  $\alpha,\beta$ -unsaturated cyclohexenone systems.

Earlier, we had reported the synthesis of some chloro-/aryl-substituted-5,5-dimethyl-2-cyclohexenones from their precursor dihalocyclohexenones. We had found the regiospecific substitution of the bromo-group when subjected to the Suzuki-Miyaura cross-coupling reaction [5].

In further continuation of our investigations of coupling reactions of compounds with differential bond strengths [6,7], we now report for the first instance of time, an alternative method for the synthesis of nine chloro- and aryl-substituted 5,5-dimethyl-2-cyclohexenones: the 2-chloro-3-aryl-5,5-dimethyl-2-cyclohexenones (**5a-i**) from the corresponding tosylate-precursor: 2-chloro-3-tosyl-5,5-dimethyl-2-cyclohexenone (**3**) in greater than 85% yields (Scheme 1).

**Table 1.** Crystal structure and refinement statistics.

Properties / Compound	3	5e	5h
CCDC	1875712	1940404	1940405
Empirical formula	C <sub>15</sub> H <sub>17</sub> ClO <sub>4</sub> S	C <sub>20</sub> H <sub>18</sub> ClFO	C <sub>12</sub> H <sub>13</sub> OSCl
Formula weight	328.80	328.79	289.78
Temperature (K)	290	296(2)	290
Crystal system	Monoclinic	Monoclinic	Triclinic
Space group	P2 <sub>1</sub> /c	P2 <sub>1</sub> /c	P-1
a (Å)	8.8687(3)	6.4900(5)	6.7517(6)
b (Å)	10.5537(4)	18.6070(13)	8.8376(9)
c (Å)	16.6862(7)	14.2146(11)	12.6049(12)
α (°)	90	90	109.538(3)
β (°)	89.807(3)	102.324(2)	98.597(3)
γ (°)	90	90	90.417(3)
Volume (Å <sup>3</sup> )	1561.78(10)	1677.0(2)	699.52(12)
Z	4	4	2
ρ <sub>calc</sub> (g/cm <sup>3</sup> )	1.398	1.309	1.376
μ (mm <sup>-1</sup> )	0.390	0.239	0.410
F(000)	688.0	688.0	302.0
Crystal size (mm <sup>3</sup> )	0.35 × 0.33 × 0.30	0.34 × 0.29 × 0.25	0.39 × 0.35 × 0.30
Radiation	MoKα (λ = 0.71073 Å)	MoKα (λ = 0.71073 Å)	MoKα (λ = 0.71073 Å)
2θ range for data collection (°)	6.716 to 54.962	6.262 to 52.224	6.114 to 59.288
Index ranges	-11 ≤ h ≤ 11 -12 ≤ k ≤ 13 -21 ≤ l ≤ 18	-8 ≤ h ≤ 8 -22 ≤ k ≤ 22 -17 ≤ l ≤ 17	-9 ≤ h ≤ 9 -12 ≤ k ≤ 12 -17 ≤ l ≤ 17
Reflections collected	13623	25575	28754
Independent reflections	3570 [R <sub>int</sub> = 0.0467, R <sub>sigma</sub> = 0.0512]	3283 [R <sub>int</sub> = 0.0494, R <sub>sigma</sub> = 0.0307]	3898 [R <sub>int</sub> = 0.0544, R <sub>sigma</sub> = 0.0349]
Data/restraints/parameters	3570/0/193	3283/0/211	3898/0/176
Goodness-of-fit on F <sup>2</sup>	1.041	1.055	1.060
Final R indexes [I ≥ 2σ (I)]	R <sub>1</sub> = 0.0452, wR <sub>2</sub> = 0.0906	R <sub>1</sub> = 0.0875, wR <sub>2</sub> = 0.1968	R <sub>1</sub> = 0.1101, wR <sub>2</sub> = 0.2374
Final R indexes [all data]	R <sub>1</sub> = 0.0612, wR <sub>2</sub> = 0.1019	R <sub>1</sub> = 0.1060, wR <sub>2</sub> = 0.2056	R <sub>1</sub> = 0.1374, wR <sub>2</sub> = 0.2481
Largest diff. peak/hole (e Å <sup>-3</sup> )	0.29/-0.33	0.29/-0.37	0.50/-0.50

**Scheme 1.** Regiospecific synthesis of 2-chloro-3-aryl-5,5-dimethyl-2-cyclohexenones (**5a-i**).

The newly synthesized compounds were purified by column chromatography and recrystallized using petroleum benzene (60–74 °C). Good quality crystals of three representative compounds which include the substrate tosylate **3** and two products: 2-chloro-3-(3'-fluoro-4'-phenyl)-phenyl-5,5-dimethyl-2-cyclohexenone (**5e**) and 2-chloro-3-(2'-benzothio phenyl)-5,5-dimethyl-2-cyclohexenone (**5h**) were obtained by slow evaporation technique and subjected to single crystal X-ray diffraction study. Their evaluation unambiguously confirms the formation of the tosylate and its regiospecific conversion into 2-chloro-3-aryl-5,5-dimethyl-2-cyclohexenones, by *ipso*-substitution of tosyl group. The Hirshfeld 3-D energy framework and *in silico* docking studies are reported.

## 2. Experimental

### 2.1. Materials and characterization

All reactions were performed using oven-dried glass apparatus. Analytical Reagent grade solvents were purchased from SD Fine Chemicals Limited and Merck; Bangalore and used without further purification. The progress of the reactions was periodically monitored by Thin Layer Chromatography analysis of aliquots (Merck 60F<sub>254</sub> precoated silica plates) at a regular interval of time. The purification of the crude compounds was done by column chromatography using silica gel (Merck, 60–120 mesh) as the stationary phase and 2:8 ethyl acetate and petroleum benzene (60–74 °C) as the mobile phase. IR spectra of the compounds were recorded using Bruker ALPHA-P instrument. GC-MS were recorded on Agilent instrument equipped with Ascentis Express C18 (50 mm × 2.1 mm × 2.7 μm) column.

<sup>1</sup>H NMR and <sup>13</sup>C NMR of the novel compounds were obtained on Bruker AC 400 spectrometer using CDCl<sub>3</sub> as solvent and tetramethylsilane as internal standard. Chemical shifts are reported in δ (ppm downfield) with reference to tetramethyl silane. Elemental analyses were carried out with a VarioMicro Cube V1.9.7 CHNS mode elemental analyzer. Melting point of the compounds isolated as solids was recorded using VEEGO melting point apparatus model: VMP-DS and remain uncorrected.

Single-crystal X-ray diffraction (XRD) data were collected at 290 K on Bruker Apex II diffractometer. The complete intensity data set was processed using SAINT software [8]. Direct method was employed to solve the structure of the compounds using SHELXS program, followed by refinement by full matrix least squares based on F<sup>2</sup> using SHELXL [9]. All non-hydrogen atoms were refined anisotropically, while hydrogen atoms were fixed at chemically allowed positions. After several cycles of refinement, the structures of molecules **3**, **5e** and **5h** were finally reduced to the Goodness-of-Fit to 1.04, 1.055, and 1.06, respectively (Table 1). All geometrical data were calculated using PLATON [10], ORTEP and packing diagrams were generated using MERCURY [11]. The bond length and bond angle values are summarized in Tables 2 and 3, which are in agreement with reported structures [12,13]. The Hirshfeld surfaces were mapped on *d*<sub>norm</sub> and electrostatic potential using a STO-3G basis set at the Hartree-Fock (HF) level of theory. The associated two-dimensional fingerprint plots were used to calculate the percentage contribution of various interatomic contacts towards the formation of three-dimensional Hirshfeld surface, using CrystalExplorer 17.5 software [14–16].

**Table 2.** Bond lengths of compounds **3**, **5e** and **5h** (Å).

Compound 3		Compound 5e		Compound 5h	
Atoms	Distance	Atoms	Distance	Atoms	Distance
S1-O3	1.4240 (16)	C11-C6	1.733 (5)	C6-C1	1.341 (3)
S1-O4	1.4248 (16)	F1-C13	1.363 (5)	C6-C5	1.497 (4)
S1-O1	1.6152 (14)	C5-C6	1.340 (6)	C16-C11	1.393 (3)
S1-C9	1.749 (2)	C5-C9	1.479 (6)	C2-C3	1.517 (3)
C11-C5	1.724 (2)	C5-C4	1.507 (6)	C2-C1	1.520 (3)
O1-C6	1.401 (2)	C13-C14	1.380 (6)	C3-C4	1.531 (4)
O2-C4	1.213 (2)	C13-C12	1.390 (6)	C3-C7	1.527 (4)
C1-C6	1.495 (3)	C12-C11	1.392 (6)	S1-C16	1.729 (2)
C1-C2	1.535 (3)	C2-C3	1.521 (7)	S1-C9	1.742 (2)
C2-C8	1.530 (3)	C20-C19	1.380 (8)	C11-C6	1.734 (2)
C2-C3	1.532 (3)	C7-C3	1.537 (7)	C10-C9	1.375 (3)
C3-C4	1.502 (3)	C12-C15	1.489 (6)	C10-C11	1.425 (3)
C4-C5	1.485 (3)	C6-C1	1.484 (7)	C3-C8	1.511 (4)
C2-C7	1.537 (3)	C14-C9	1.396 (6)	C5-O1	1.222 (3)
C5-C6	1.334 (3)	C10-C11	1.380 (7)	C5-C4	1.491 (4)
C9-C14	1.377 (3)	C10-C9	1.392 (6)	C9-C1	1.465 (3)
C9-C10	1.383 (3)	C1-O1	1.208 (6)	C6-C1	1.341 (3)
C10-C11	1.381 (3)	C1-C2	1.498 (7)	C6-C5	1.497 (4)
C11-C12	1.383 (3)	C15-C16	1.374 (7)	C2-C3	1.517 (3)
C12-C13	1.386 (3)	C15-C20	1.410 (7)	C2-C1	1.520 (3)
C12-C15	1.503 (3)	C3-C8	1.531 (7)	C3-C4	1.531 (4)
C13-C14	1.386 (3)	C4-C3	1.517 (6)	C3-C7	1.527 (4)

**Table 3.** Bond angles of compounds **3**, **5e** and **5h** (°).

Compound 3		Compound 5e		Compound 5h	
Atoms	Angle	Atoms	Angle	Atoms	Angle
O3-S1-O4	120.14 (10)	C6-C5-C9	125.1 (4)	C16-S1-C9	91.94 (11)
O3-S1-O1	109.55 (9)	C6-C5-C4	120.0 (4)	C9-C10-C11	113.5 (2)
O4-S1-O1	102.02 (9)	C9-C5-C4	114.9 (4)	C13-C14-C15	121.5 (2)
O3-S1-C9	109.77 (10)	F1-C13-C14	116.9 (4)	C5-C4-C3	112.27 (19)
O4-S1-C9	110.19 (10)	F1-C13-C12	119.0 (4)	C10-C9-C1	123.9 (2)
O1-S1-C9	103.69 (9)	C14-C13-C12	124.1 (4)	C10-C9-S1	110.99 (16)
C6-O1-S1	121.56 (12)	C13-C12-C11	115.0 (4)	C1-C9-S1	125.07 (17)
C6-C1-C2	112.63 (16)	C13-C12-C15	125.2 (4)	C1-C6-C5	123.7 (2)
C8-C2-C3	109.54 (17)	C11-C12-C15	119.8 (4)	C1-C6-C11	122.68 (19)
C8-C2-C1	109.25 (17)	C5-C6-C1	123.3 (4)	C5-C6-C11	113.61 (18)
C3-C2-C1	107.80 (17)	C5-C6-C11	122.3 (4)	C11-C16-C15	121.0 (2)
C8-C2-C7	108.81 (18)	C1-C6-C11	114.4 (4)	C11-C16-S1	111.57 (16)
C3-C2-C7	110.46 (17)	C13-C14-C9	119.5 (4)	C15-C16-S1	127.41 (19)
C1-C2-C7	110.96 (17)	C19-C20-C15	119.4 (5)	C3-C2-C1	116.16 (19)
C4-C3-C2	112.57 (17)	C11-C10-C9	121.0 (4)	C16-C11-C12	120.1 (2)
O2-C4-C5	121.8 (2)	O1-C1-C6	122.0 (5)	C16-C11-C10	112.0 (2)
O2-C4-C3	123.39 (19)	O1-C1-C2	122.6 (5)	C12-C11-C10	127.9 (2)
C5-C4-C3	114.83 (18)	C6-C1-C2	115.4 (4)	C2-C3-C4	107.5 (2)
C6-C5-C4	121.3 (2)	C16-C15-C20	118.4 (5)	C2-C3-C7	111.53 (19)
C6-C5-C11	122.03 (17)	C16-C15-C12	119.9 (5)	C4-C3-C7	110.1 (2)
C4-C5-C11	116.66 (15)	C20-C15-C12	121.7 (4)	C2-C3-C8	108.4 (2)
C5-C6-O1	117.68 (19)	C10-C9-C14	117.8 (4)	C4-C3-C8	110.0 (2)
C5-C6-C1	123.88 (19)	C10-C9-C5	120.2 (4)	C7-C3-C8	109.4 (2)
O1-C6-C1	118.12 (17)	C14-C9-C5	122.0 (4)	O1-C5-C4	122.9 (2)
C14-C9-C10	121.6 (2)	C5-C4-C3	115.2 (4)	O1-C5-C6	120.6 (2)
C14-C9-S1	118.81 (17)	C1-C2-C3	113.4 (4)	C4-C5-C6	116.5 (2)
C10-C9-S1	119.57 (17)	C2-C3-C4	108.2 (4)	C6-C1-C9	127.4 (2)
C11-C10-C9	118.3 (2)	C2-C3-C8	109.6 (4)	C16-C15-C14	118.8 (2)
C11-C12-C15	120.4 (2)	C4-C3-C8	109.6 (4)	C14-C13-C12	121.1 (2)
C13-C12-C15	120.9 (2)	C2-C3-C7	109.0 (4)	C6-C1-C2	117.7 (2)
C14-C13-C12	120.8 (2)	C4-C3-C7	111.4 (4)	C9-C1-C2	114.95 (18)
C9-C14-C13	119.0 (2)	C8-C3-C7	109.1 (5)	C13-C12-C11	117.5 (2)

The interaction energies in a molecule, resulting in the formation of three-dimensional architecture of a crystal, were calculated using CrystalExplorer17.5 software [17,18]. The software was also used to calculate interaction energies in the representative crystals of compounds **3**, **5e** and **5h**.

Crystallographic structure of 121p (H-ras) protein with a resolution of 1.54 Å was obtained from protein data bank (PDB). The heteroatom and ligand data were removed from the protein pdb file and used for further docking studies. The novel molecules **5e** and **5h** were taken as ligands. Ligand and protein molecules were converted into pdbqt format in PyRx 0.8 docking tool, with a built-in Vina wizard [19]. The protein and ligand were docked with a grid box size of 42.1, 39.87, 43.82 Å and grid centre 5.86, 25.15 and 11.93 Å. The atomic interactions and electrostatic maps of the ligands were calculated using the autogrid module. Out of several possible interactions, the complex with lowest binding energy was considered for ligand-

protein docking studies. Molecular graphics laboratory (MGL) tools were used to analyze the results from Vina Wizard and the best conformation with lowest binding energy was exported for 2D plot generation using Ligplot+ [20]. The docking conformation of the best complex was represented using PyMOL [5].

## 2.2. Synthesis and analytical data

### 2.2.1. Synthesis of 2-chloro-3-tosyl-5,5-dimethyl-2-cyclohexenone (3)

To a solution of 2-chloro-5,5-dimethyl-1,3-cyclohexanedione (**2**, 11.49 mmole) and triethylamine (2.32 g, 22.988 mmole) in 30 mL THF, stirred at room temperature, was added *p*-toluenesulfonylchloride (*p*-TsCl, 2.5 g, 13.157 mmole) over a period of 1 hour. After completion of addition, the reaction mixture was heated to reflux and the progress of the reaction

was periodically monitored by TLC analysis of small aliquots at regular intervals of time. After the complete conversion was indicated by disappearance of starting material on TLC, the reaction mixture was diluted with water and extracted with ethylacetate (3 × 20 mL). The organic layer was separated, washed with water (3 × 20 mL), brine solution (3 × 20 mL) and purified by column chromatography using 2:8 ethyl acetate: petroleum benzene (60-74 °C) as mobile phase and silica gel (100-200 mesh) as stationary phase to isolate 3.6 g of 2-chloro-3-tosyl-5,5-dimethyl-2-cyclohexenone (**3**) (Scheme 1).

**2-Chloro-3-tosyl-5,5-dimethyl-2-cyclohexenone (3):** Color: White. Yield: 96%. M.p.: 196-198 °C. FT-IR (KBr,  $\nu$ ,  $\text{cm}^{-1}$ ): 2959, 2931, 2877, 1698, 1613, 1369, 1341, 1266, 1177, 1141, 1089, 1018, 988, 947, 915, 809, 737, 668, 637, 597, 565, 547.  $^1\text{H}$  NMR (400 MHz,  $\text{CDCl}_3$ ,  $\delta$ , ppm): 1.12 (s, 6H, 2CH<sub>3</sub>), 2.44 (s, 2H, CH<sub>2</sub>-C=C), 2.51 (s, 3H, Ar-CH<sub>3</sub>), 2.83 (s, 2H, CH<sub>2</sub>-CO), 7.38 (d, 2H,  $J$  = 8 Hz, Ar), 7.88 (d, 2H,  $J$  = 8 Hz, Ar).  $^{13}\text{C}$  NMR (100 MHz,  $\text{CDCl}_3$ ,  $\delta$ , ppm): 21.7 (2CH<sub>3</sub>), 27.8 (CCH<sub>3</sub>), 27.9 (ArCH<sub>3</sub>), 32.7 (CH<sub>2</sub>-C=C), 51.0 (CH<sub>2</sub>-CO), 122.1 (Ar), 128.3 (Ar), 130.0 (Ar), 132.9 (Ar), 146.3 (C-O), 160.6 (CCI), 191.2 (CO). MS (EI,  $m/z$  (%)): 329 (M<sup>+</sup>, 100). Anal. calcd. for C<sub>15</sub>H<sub>17</sub>ClO<sub>4</sub>S: C, 54.79; H, 5.21; S, 9.75. Found: C, 54.68; H, 5.18; S, 9.72%. CCDC number: 1875712.

**2-Chloro-3-(3'-fluoro-4'-phenyl)-phenyl-5, 5-dimethyl-2-cyclohexenone (5e):** Color: White. Yield: 94%. M.p.: 82-84 °C. FT-IR (KBr,  $\nu$ ,  $\text{cm}^{-1}$ ): 2962, 2925, 2870, 1677, 1613, 1554, 1482, 1402, 1343, 1306, 1242, 1129, 998, 966, 839, 771, 722, 701, 647, 578, 559, 481, 455.  $^1\text{H}$  NMR (400 MHz,  $\text{CDCl}_3$ ,  $\delta$ , ppm): 1.19 (s, 6H, 2CH<sub>3</sub>), 2.49 (s, 2H, CH<sub>2</sub>-C=C), 2.82 (s, 2H, CH<sub>2</sub>-CO), 7.01 (d, 2H,  $J$  = 7.6 Hz, Ar-H), 7.38 (d, 1H,  $J$  = 7.2 Hz, Ar-H), 7.42-7.46 (m, 3H, Ar-H), 7.58 (d, 2H,  $J$  = 7.6 Hz, Ar-H).  $^{13}\text{C}$  NMR (100 MHz,  $\text{CDCl}_3$ ,  $\delta$ , ppm): 28.0 (CH<sub>3</sub>), 33.3 (C), 49.1 (CH<sub>2</sub>-C=C), 51.2 (CH<sub>2</sub>-CO), 117.6 (Ar), 117.9 (Ar), 125.9 (Ar), 127.7 (Ar), 128.4 (Ar), 128.6 (Ar), 129.1 (Ar), 130.3 (Ar), 134.4 (Ar), 134.5 (Ar), 135.6 (Ar), 136.5 (C-O), 153.2 (CCI), 195.3 (CO). MS (EI,  $m/z$  (%)): 329 (M<sup>+</sup>, 100). Anal. calcd. for C<sub>20</sub>H<sub>18</sub>ClFO: C, 73.06; H, 5.52. Found: C, 72.96; H, 5.41%. CCDC number: 1940404.

**2-Chloro-3-(2'-benzothiophenyl)-5, 5-dimethyl-2-cyclohexenone (5h):** Color: White solid. Yield: 91%. M.p.: 101-103 °C. FT-IR (KBr,  $\nu$ ,  $\text{cm}^{-1}$ ): 3015, 2961, 2929, 1679, 1412, 1344, 1271, 1215, 1155, 1115, 854, 833, 743, 666, 587, 508, 430.  $^1\text{H}$  NMR (400 MHz,  $\text{CDCl}_3$ ,  $\delta$ , ppm): 1.18 (s, 6H, 2CH<sub>3</sub>), 2.51 (s, 2H, CH<sub>2</sub>-C=C), 2.85 (s, 2H, CH<sub>2</sub>-CO), 7.33-7.34 (m, 3H, Ar-H), 7.77-7.81 (m, 2H, Ar-H).  $^{13}\text{C}$  NMR (100 MHz,  $\text{CDCl}_3$ ,  $\delta$ , ppm): 28.1 (CH<sub>3</sub>), 33.2 (CH<sub>3</sub>), 49.7 (C), 51.2 (CH<sub>2</sub>-C=C), 53.4 (CH<sub>2</sub>-CO), 122.0 (Ar), 123.9 (Ar), 124.1 (Ar), 124.5 (Ar), 126.3 (Ar), 131.5 (Ar), 133.5 (Ar), 139.1 (C-O), 154.8 (CCI), 194.7 (CO). MS (EI,  $m/z$  (%)): 291 (M<sup>+</sup>, 100). Anal. calcd. for C<sub>16</sub>H<sub>15</sub>ClOS: C, 66.08; H, 5.20; S, 11.03%. Found: C, 65.87; H, 5.13; S, 10.89%. CCDC number: 1940405.

### 2.2.2. General procedure for the preparation of 2-chloro-3-aryl-5,5-dimethyl-2-cyclohexenones (5a-i)

A suspension of 2-chloro-3-tosyl-5,5-dimethyl-2-cyclohexenone (**3**, 0.5 g, 2.11 mmole), aryl boronic acid (**4a-i**, 1.1 mmolar equivalent), Pd(OAc)<sub>2</sub> catalyst (10 mg, 0.044 mmoles, 0.21 mol%), PPh<sub>3</sub> (50 mg, 0.19 mmoles) and K<sub>3</sub>PO<sub>4</sub> (0.87 g, 4.09 mmoles) in 5 mL of 1,4-dioxane were taken in a 15 mL Sigma-Aldrich Ace pressure tube along with a magnetic pellet, purged with N<sub>2</sub> gas and sealed. The pressure tube was introduced into a preheated oil bath at 110 °C and magnetically stirred for a period of 4-8 hours. After complete conversion of reactants as indicated by TLC analysis, the reaction was allowed to attain ambient temperature, transferred to a beaker, and diluted with ethyl acetate (20 mL). The extract was filtered over a bed of Celite® and washed with ethyl acetate (20 mL). The combined filtrate was concentrated on a rotary evaporator and the crude product was purified by column chromatography using silica gel (Merck, 60-120 mesh) as the stationary phase and ethyl acetate: petroleum benzene (60-74 °C) in the ratio 2:8 as mobile

phase to isolate the compounds 2-chloro-3-aryl-5,5-dimethyl-2-cyclohexenones **5a-i** in greater than 80% yield (Scheme 1).

## 3. Results and discussions

5,5-Dimethyl-1,3-cyclohexanedione (**1**) was sequentially converted to 2-chloro-5,5-dimethyl-2,3-cyclohexanedione (**2**) by reaction with *N*-chlorosuccinimide (NCS) in CHCl<sub>3</sub> [5]. Compound **2** on heating with *p*-toluenesulfonylchloride (*p*-TsCl) with triethylamine (TEA) in THF furnished the novel organotosylate: 2-chloro-3-tosyl-5, 5-dimethyl-2-cyclohexenone (**3**).

The compound **3** is a suitable substrate for Suzuki-Miyaura cross-coupling reaction, with two possible reaction sites: the carbon bearing the chlorine and the carbon bearing the tosyl-group. Hence, as trial reaction **3** was subjected to Suzuki-Miyaura cross-coupling reaction with 2-methoxyphenyl boronic acid (**4a**), using different palladium catalysts: Pd(PPh<sub>3</sub>)<sub>4</sub>, Pd(OAc)<sub>2</sub> and Pd(dppf)<sub>2</sub>Cl<sub>2</sub>, in the presence of differing bases: K<sub>2</sub>CO<sub>3</sub>/Na<sub>2</sub>CO<sub>3</sub> and K<sub>3</sub>PO<sub>4</sub> in DMF/1,4-dioxane/THF solvents. Out of several catalytic systems used, the best results with respect to reaction duration and isolated yields of mono-arylated product 2-chloro-3-(2'-methoxy)phenyl-5,5-dimethyl-2-cyclohexenone (**5a**) was obtained by employing Pd(OAc)<sub>2</sub> (44  $\mu$ mole), PPh<sub>3</sub> (0.19 mmole), K<sub>3</sub>PO<sub>4</sub> (4.09 mmole) in 5 mL 1,4-dioxane solvent at 110 °C under nitrogen atmosphere. The reaction conditions were further optimized and eight different aryl boronic acids (**4b-i**) were reacted with compound **3** under the same reaction conditions to obtain compounds **5b-i** in greater than 85% isolated yields. Each reaction was carried for a minimum of three trials and the optimized yields and reaction durations are given in Table 4. Formation of products **5a-i** confirms the regiospecific nature of the reaction due to differential carbon-chlorine and carbon-tosyl bond strengths.

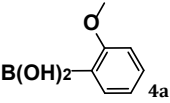
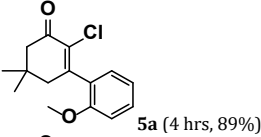
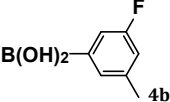
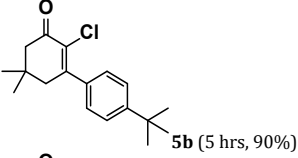
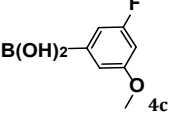
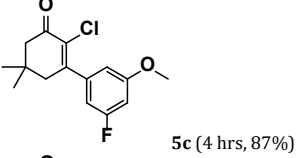
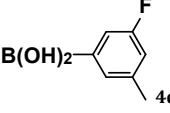
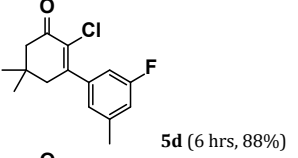
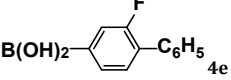
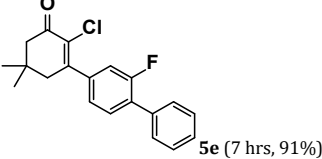
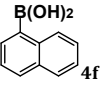
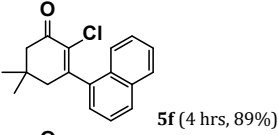
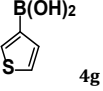
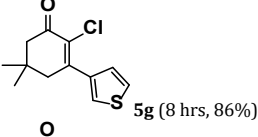
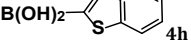
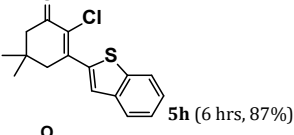
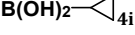
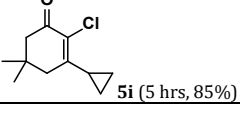
### 3.1. Mechanism

In general,  $\alpha,\beta$ -unsaturated ketones are well recognized to be polarized with the separation of a discrete negative charge on the oxygen and corresponding positive charge on the  $\beta$ -vinylic carbon. In the reactant molecule **3**, this renders the carbon-tosylate bond to cleave easily, rendering the tosylate group to become a good leaving group [21]. Further, the present study, in comparison to our earlier report [5] clearly indicates that between the bromo and the tosylate substituents, the reactivity of the tosylate group is slightly lesser when compared to the bromo substituent. The tosylate group, under the conditions employed by us takes a rather longer duration of time for completion of the reaction in comparison to the bromo-analogue, indicating that even though the tosyl group is a good leaving group, it has reactivity lesser than the bromo-group in terms of leaving group capacity. These results are in good concordance with the recent findings of other scientists. Therefore, all these studies indicate that the reactivity of leaving groups is bromo > triflate > tosylate > chloro [22]. The rest of the reaction mechanistic cycle for our reactions, we postulate that to traverse through accepted routes reported by other scientists for the Suzuki-Miyaura cross-coupling reaction [3,5,23].

### 3.2. Crystal and molecular structure description

Good quality crystals of three representative compounds: 2-chloro-3-tosyl-5,5-dimethyl-2-cyclohexenone (**3**), 2-chloro-3-(3'-fluoro-4'-phenyl)-phenyl-5,5-dimethyl-2-cyclohexenone (**5e**) and 2-chloro-3-(2'-benzothiophenyl)-5, 5-dimethyl-2-cyclohexenone (**5h**) were obtained by slow evaporation method in AR grade petroleum benzene solvent and subjected to single-crystal XRD studies.

**Table 4.** 2-Chloro-3-aryl-5,5-dimethyl-2-cyclohexenones (**5a-i**).

Entry	Boronic acids	2-Chloro-3-aryl-5,5-dimethyl-2-cyclohexenones (Reaction duration and % yields)
1	 <b>4a</b>	 <b>5a</b> (4 hrs, 89%)
2	 <b>4b</b>	 <b>5b</b> (5 hrs, 90%)
3	 <b>4c</b>	 <b>5c</b> (4 hrs, 87%)
4	 <b>4d</b>	 <b>5d</b> (6 hrs, 88%)
5	 <b>4e</b>	 <b>5e</b> (7 hrs, 91%)
6	 <b>4f</b>	 <b>5f</b> (4 hrs, 89%)
7	 <b>4g</b>	 <b>5g</b> (8 hrs, 86%)
8	 <b>4h</b>	 <b>5h</b> (6 hrs, 87%)
9	 <b>4i</b>	 <b>5i</b> (5 hrs, 85%)

The compounds 2-chloro-3-tosyl-5,5-dimethyl-2-cyclohexenone (**3**) and 2-chloro-3-(3'-fluoro-4'-phenyl)-phenyl-5,5-dimethyl-2-cyclohexenone (**5e**) crystallize in monoclinic system ( $P2_1/c$ ). However, 2-chloro-3-(2'-benzothiophenyl)-5,5-dimethyl-2-cyclohexenone (**5h**) crystallizes in triclinic system ( $P-1$ ). The molecular view of compounds **3**, **5e** and **5h** are given in Figure 1. The crystal structure and refinement details for the compounds **3**, **5e** and **5h** are summarized in Table 1. In compound **3**, the Cg1 [ring centroid of C1/C6] is puckered at C2 and exhibits nearly an *envelope* conformation of the type  $E_2$ , with puckering amplitude  $Q = 0.490$  Å, pseudo-rotation angle  $\theta = 53.1(2)^\circ$  and the relative phase angle  $\varphi = 78.8(3)^\circ$ . In molecule **5e**, the Cg1 phenyl ring is puckered at C3 displaying nearly an *envelope* conformation of the type  $^1E$  with total puckering amplitude  $Q = 0.462(6)$  Å, pseudo-rotation angle  $\theta = 52.3(6)^\circ$  and the relative phase angle  $\varphi = 105.5(9)^\circ$ . However, in compound **5h**, the Cg2 [ring centroid of C1/C6] is

puckered at C3 and adopts *half-chair* conformation with the total puckering amplitude of  $Q = 0.473(3)$  Å, pseudo-rotation angle  $\theta = 50.3(4)^\circ$  and the relative phase angle of  $\varphi = 131.2(4)^\circ$  [24, 25]. The puckering amplitudes are in agreement with the cyclohexenone ring of the compound  $C_{14}H_{15}ClO$  and  $C_{15}H_{17}ClO_2$  [26,27].

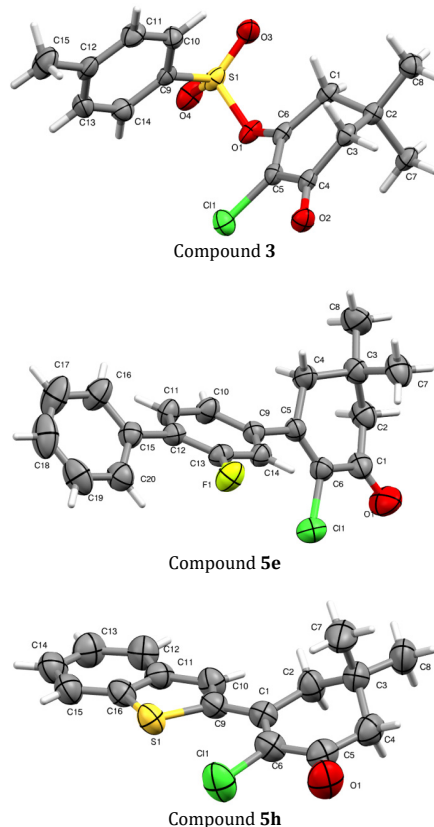
In compound **3**, the Cg1 and Cg2 [ring centroid of C9/C14] planes are inclined to each other about the central  $-SO_3$  group with the dihedral angle of  $62.38(9)^\circ$ . The S1 atom in the central part of the structure exhibits distorted trigonal geometry, confirmed by the bond angle values of  $O4-S1-O3=120.14^\circ$ ,  $O3-S1-O1=109.54^\circ$  and  $O4-S1-O1=102.02^\circ$ . In molecule **5e**, the Cg1 plane makes a dihedral angle of  $57.82^\circ$  and  $24.03^\circ$  with Cg2 [ring centroid of C9/C14] and Cg3 [ring centroid of C15/C20] planes, respectively.

**Table 5.** Hydrogen bonding geometry ( $\text{\AA}$ ,  $^\circ$ ).

Compound	D-H...A	D-H	H...A	D...A	$\angle$ D-H...A	Symmetry code
3	C10-H10...O4	0.93	2.58	3.433	154	1-x, -1/2+y, 1/2-z
	C11-H11...O2	0.93	2.58	3.371	143	-1+x, y, z
	C3-H3A...O1	0.93	2.62	3.437	143	2-x, 1/2+y, 1/2-z
5e	C11-H11...Cl1 <sup>#</sup>	0.93	2.84	3.634	144	1-x, 1-y, 1-z
	C20-H20...F1*	0.93	2.47	2.928	111	
5h	C8-H8A...O1	0.93	2.72	3.606	165	-1+x, y, z

<sup>#</sup> Weak intermolecular interaction.

\* Intramolecular interaction.

**Figure 1.** Labeled ORTEP drawn at 50% of probability for the molecules **3**, **5e**, and **5h**.

The plane of central fluorophenyl ring Cg2 makes the dihedral angle of  $35.09^\circ$  with Cg3 plane, indicating more twist between the planes of Cg1 and Cg2, due to electrostatic repulsion of hydrogen atoms on the ring systems. In molecule **5h**, the Cg2 plane makes a dihedral angle of  $22.90^\circ$  with Cg4 [ring centroid of S1-C9/C16].

The packing diagrams for molecules **3**, **5e**, and **5h** are depicted in Figure 2. The crystal structure of compound **3** is stabilized by intermolecular hydrogen bonding interactions of the type C3-H3A...O1, C10-H10...O4 and C11-H11...O2 connecting the molecules in the form of one-dimensional polymeric chains propagating infinitely along crystallographic *b*-axis (i), while these interactions generate the layer stacking appearance along crystallographic *a*-axis (ii). In the crystal structure of molecule **5e**, the packing of molecules was established by a weak intermolecular interaction of the type C11-H11...Cl1 incorporating a graph set of  $R_2^2(14)$  ring motif. Besides this, there is an intramolecular interaction between C20-H20...F1 (Table 5) incorporating an  $S(6)$  closed ring motif. In molecule **5h**, the molecules are linked in the form of head-to-tail pattern through weak intermolecular interactions of the type C8-H8A...O1 to form one-dimensional independent polymeric chains propagating infinitely along crystallographic *b*-axis. The hydrogen bonding and interactions present in molecules **3**, **5e**, and **5h** are given in Table 5.

### 3.3. Hirshfeld surfaces and two-dimensional fingerprint calculations

The three-dimensional Hirshfeld surfaces were mapped on  $d_{norm}$  and electrostatic potential for the compounds **3**, **5e** and **5h**, with the following area and volume: 335.11, 357.45, 304.41  $\text{\AA}^2$  and 383.93, 412.37, 343.47  $\text{\AA}^3$ , respectively. The Hirshfeld surfaces for all the compounds were obtained in transparent mode to visualize atoms and functional groups involved in the molecular structures, as shown in Figure 3. The intermolecular interactions (Table 5) involved in the crystal packing of the compounds **3**, **5e**, and **5h** were investigated. In the given orientations of Hirshfeld surfaces mapped on  $d_{norm}$  the reader can notice the donor parts of intermolecular interactions listed in Table 5. The bright red coloured circular spots labelled as 1, 2 and 3 on  $d_{norm}$  of compound **3** reveals the donor parts of intermolecular C10-H10...O4, C11-H11...O2 and C3-H3A...O1 interactions respectively. Fortunately, on the posture of  $d_{norm}$  surface of compound **5e**, both, the donor and acceptor regions of weak intermolecular C11-H11...Cl1 interaction are seen at the bright red colored regions labelled as 1 and 2 respectively. Whereas, only the donor part (labelled as 1) of intermolecular C8-H8A...O1 interaction is visualized on the  $d_{norm}$  of compound **5h**.

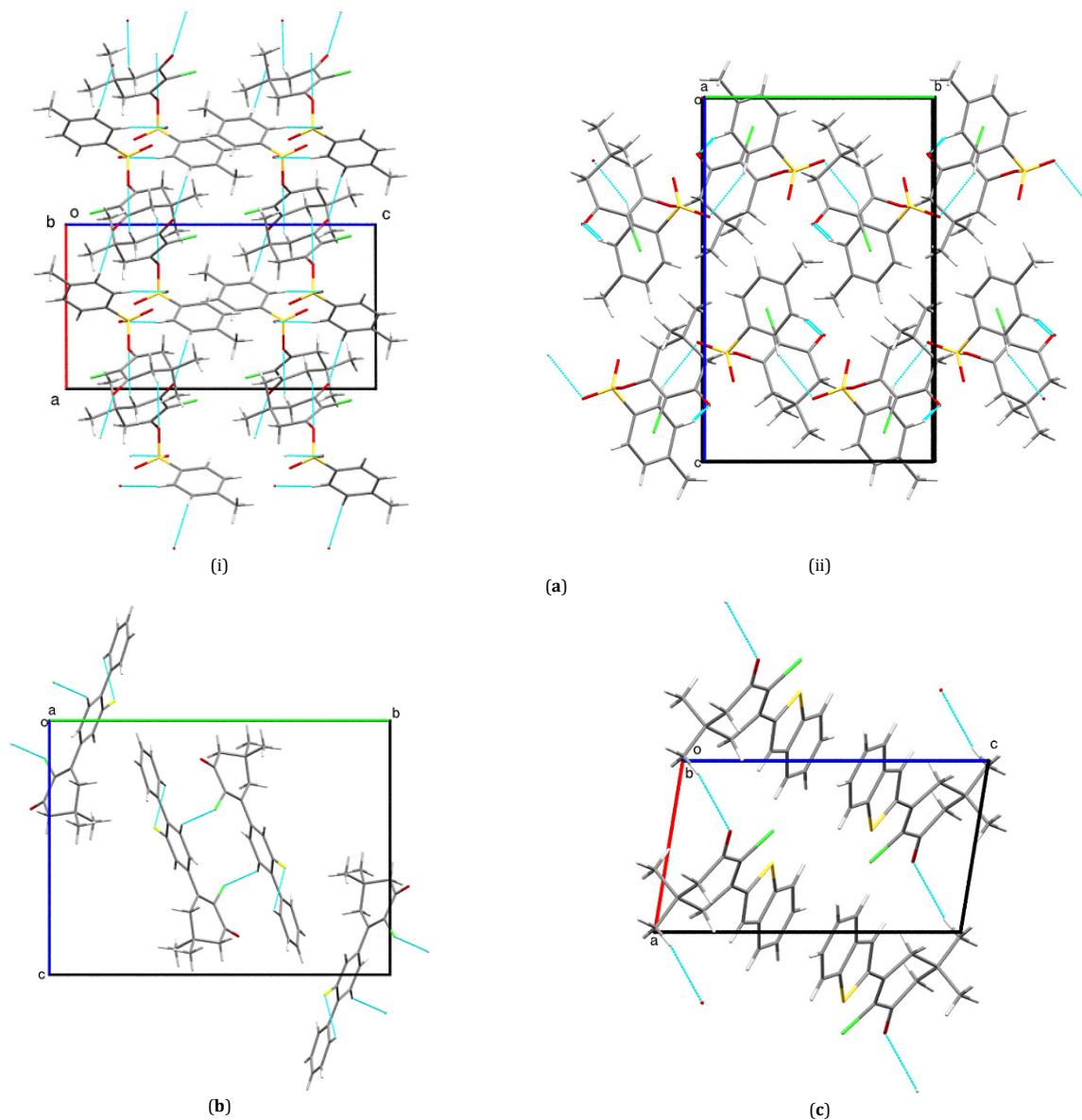


**Figure 2.** (a) Packing of molecules in compound **3** (i) and (ii) viewed along *b* and *a* axes. The cyan-colored dotted lines are hydrogen bonding interactions. (b) Packing of molecules in compound **5e** viewed along *a* axis. The cyan-colored dashed lines indicate intermolecular C11-H11...Cl1 and intra-molecular C20-H20...F1 interactions. (c) Packing of molecules in compound **5h** viewed along the *b* axis. The cyan colored dashed lines indicate intermolecular C8-H8A...O1 interactions.

Further, in the same way, the similar donor and acceptor regions of intermolecular interactions incurred in the crystal packing of the compounds **3**, **5e** and **5h** are recognized as blue and red colored patches on the Hirshfeld surfaces mapped on electrostatic potentials. The presence of other blue and red colored patches on it demonstrates the positions of electro positive and negative elements of the molecules [28].

The two-dimensional fingerprint plots for molecules **3**, **5e** and **5h** are given in Figure 4. The results of the compound **3** showed the inter-contacts H...O, H...H, H...C, and H...Cl have the following contribution 36.3, 33.9, 14.3 and 13.4%, respectively. This indicate, in compound **3**, the H...O pairs of contacts have been recorded as the predominant contribution towards the formation of a three-dimensional Hirshfeld surface, which agrees with C-H...O interactions. In the compound **5e**, the H...H, H...C, H...O, H...Cl and H...F inter contacts have contributed 42.4%, 22.6%, 10.5%, 10.3% and 9.3% respectively. The contribution of H...C and H...Cl to the Hirshfeld surface in compound **5e** reflects the presence of weak intermolecular

C11-H11...Cl1 interaction. Whereas, in compound **5h**, the inter-contacts H...H, H...C, H...Cl, H...O and H...S have contributed 41.7, 14.5, 14.4, 11.8 and 9.7%, respectively, further the H...C and H...O contributions due to the presence of intermolecular C8-H8A...O1 interaction. In the compounds **5e** and **5h** the H...H pair of contacts is the major contribution.

### 3.4. Three-dimensional interaction energies

The crystal packing with stabilized interactions is visualized and analysed using qualitative energy framework analysis. In this method, we calculated the interaction energy between the various molecular pairs and generated a three-dimensional topology of the dominant interactions in molecular crystal packing of the compounds **3**, **5e** and **5h**. The total interaction energies of the compounds **3**, **5e** and **5h** were resolved into  $E_{ele}$ ,  $E_{dis}$ ,  $E_{pot}$ , and  $E_{rep}$  components.

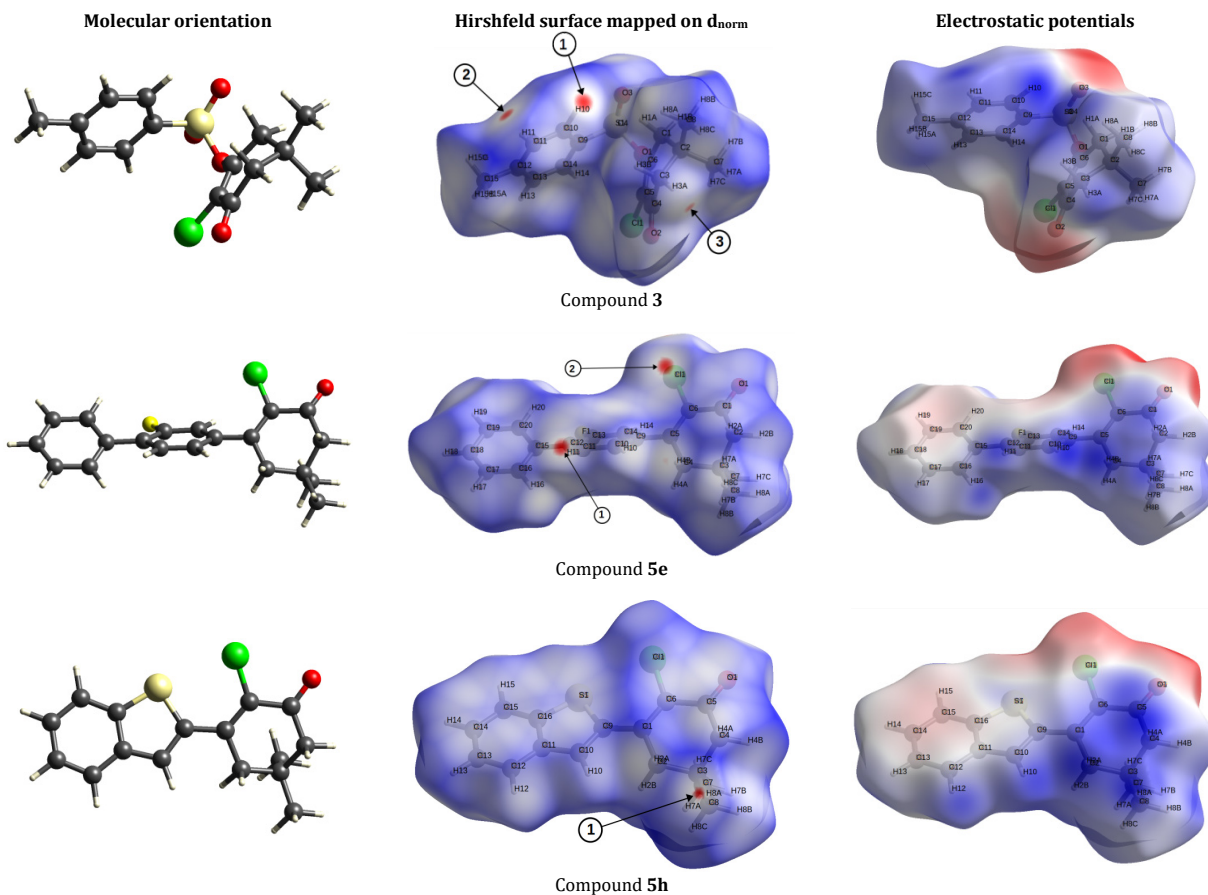


**Figure 3.** The Hirshfeld surfaces mapped on  $d_{norm}$  and electrostatic potentials for molecules **3**, **5e**, and **5h** compounds. The bright red color spots on  $d_{norm}$  of each molecule indicates intermolecular interactions. The red and blue regions on electrostatic potentials represent the corresponding electrostatic negative acceptor and positive donor potentials involved in intermolecular interactions.

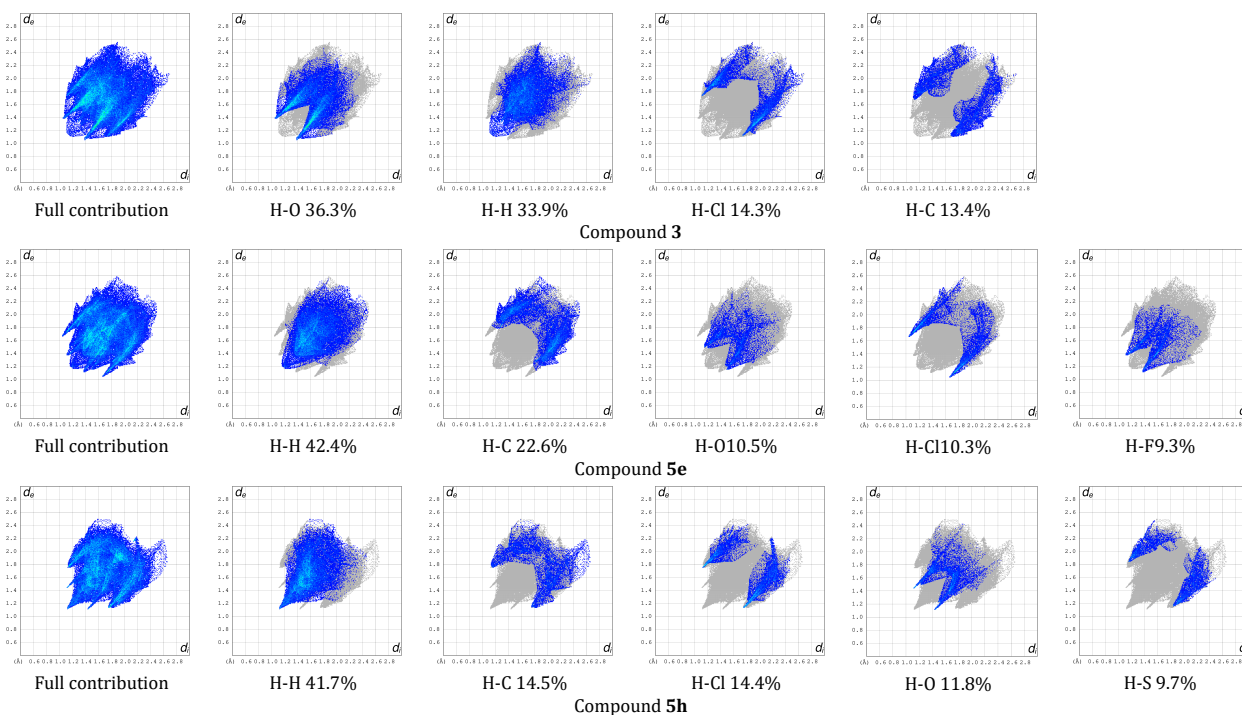


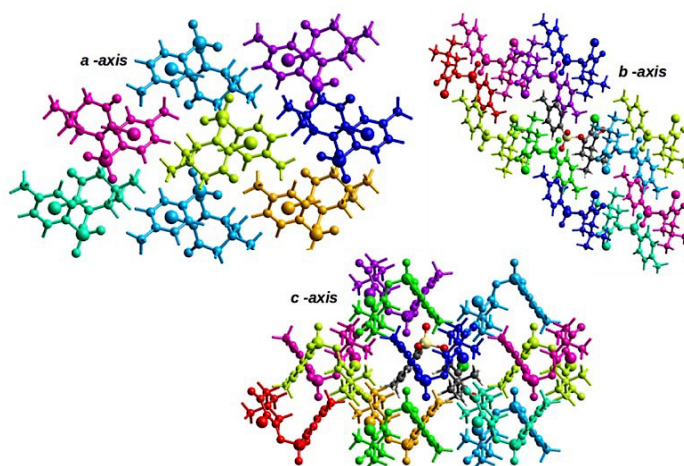
**Figure 4.** The fingerprint plots compound **3**, compound **5e**, and compound **5h** compounds. The grey-coloured pattern indicates the outline of the full fingerprint. The  $d_e$  and  $d_i$  along  $y$  and  $x$  axes are the closest nuclei external and internal to the three-dimensional Hirshfeld surface [29].



**Table 6.** Interaction energies (kJ/mol), R is the distance between molecular centroids (mean atomic position) in Å. Total energies, only reported for two benchmarked energy models, are the sum of the four energy components, scaled appropriately (see the scale factor table below) for compound 3.

Color code	N	Symmetry	R	Electron density	$E_{ele}$	$E_{pol}$	$E_{dis}$	$E_{rep}$	$E_{tot}$
Red	1	-x, -y, -z	14.43	B3LYP/6-31G(d,p)	1.9	-0.2	-1.3	0.0	0.7
Orange	1	-x, -y, -z	8.20	B3LYP/6-31G(d,p)	-10.9	-4.3	-46.6	32.1	-35.5
Yellow	2	x, y, z	8.87	B3LYP/6-31G(d,p)	-7.8	-2.4	-14.2	9.2	-16.7
Light Green	2	-x, y+1/2, -z+1/2	6.77	B3LYP/6-31G(d,p)	-11.1	-4.7	-34.0	23.8	-30.1
Green	1	-x, -y, -z	12.87	B3LYP/6-31G(d,p)	0.9	-0.3	-7.2	1.9	-4.4
Cyan	2	-x, y+1/2, -z+1/2	7.93	B3LYP/6-31G(d,p)	-13.2	-4.8	-31.7	22.3	-31.4
Blue	2	x, -y+1/2, z+1/2	8.38	B3LYP/6-31G(d,p)	-8.4	-2.5	-24.0	17.7	-20.7
Purple	1	-x, -y, -z	9.17	B3LYP/6-31G(d,p)	-12.0	-2.6	-12.3	5.2	-22.1
Pink	2	x, -y+1/2, z+1/2	12.22	B3LYP/6-31G(d,p)	-0.3	-0.3	-6.2	1.3	-5.2

Energy Model (30)	$K_{ele}$	$K_{pol}$	$K_{disp}$	$K_{rep}$
CE-HF ... HF/3-21G electron densities	1.019	0.651	0.901	0.811
CE-B3LYP ... B3LYP/6-31G(d,p) electron densities	1.057	0.740	0.871	0.618

**Figure 5.** The color-coding pattern of molecules surrounding the original molecule in a cluster of molecule 3 within the default radius of 3.8 Å, when it is viewed along crystallographic *a*, *b* and *c* axes. The color-coding scheme and their interaction energies in component form is given in Table 6.

The three-dimensional interaction energy profiles of Coloumbic dispersion and total energy components were constructed for the title compounds using default red, green, and blue-colored tubes. The variation of thickness of solid cylinders mapping the molecules in each energy frame works to indicate the relative strength of interaction between the molecules, which are also confirmed by their noticeable higher negative energy values are given in Tables 6-8 and energy values are given in Figures 5, 6 and 7. In each profile of the title compounds 3, 5e and 5h, the tube size was maintained as 150 with 10kJ/mol cut-off energy values to avoid mapping of weak interactions and for clarity purpose they are depicted in Figure 8-10.

In the cluster of 3 molecules, the maximum total interaction energy was  $E_{tot} = -35.5$  kJ/mol [ $E_{ele} = -10.9$  kJ/mol;  $E_{pol} = -4.3$  kJ/mol;  $E_{dis} = -46.69$  kJ/mol and  $E_{rep} = 32.1$  kJ/mol] with the molecule interacting at the molecular centroid distance of  $R = 8.20$  Å. The other higher total interaction energy  $E_{tot} = -31.4$  was observed for the molecules interacting at  $R = 7.93$  Å [ $E_{ele} = -13.2$  kJ/mol;  $E_{pol} = -4.8$  kJ/mol;  $E_{dis} = -31.7$  kJ/mol and  $E_{rep} = 22.3$  kJ/mol].

The stabilization of 5e molecules, in which the highest total interaction energy  $E_{tot} = -53.8$  kJ/mol [ $E_{ele} = -18.7$  kJ/mol;  $E_{pol} = -4.6$  kJ/mol;  $E_{dis} = -59.4$  kJ/mol and  $E_{rep} = 34.0$  kJ/mol] was observed for the molecule interacting at  $R = 4.68$  Å. The least

total interaction energy  $E_{tot} = -2.3$  kJ/mol [ $E_{ele} = -0.7$  kJ/mol;  $E_{pol} = -0.1$  kJ/mol;  $E_{dis} = -3.6$  kJ/mol and  $E_{rep} = 0.3$  kJ/mol] in the cluster was found with the two molecules interacting at  $R = 14.31$  Å.

In the cluster of 5h molecules, the maximum total interaction energy was  $E_{tot} = -27.5$  kJ/mol [ $E_{ele} = -2.9$  kJ/mol;  $E_{pol} = -1.4$  kJ/mol;  $E_{dis} = -42.0$  kJ/mol and  $E_{rep} = 21.4$  kJ/mol] interacting at  $R = 7.74$  Å and it is observed as least  $E_{tot} = -3.1$  kJ/mol [ $E_{ele} = 0.7$  kJ/mol;  $E_{pol} = -0.3$  kJ/mol;  $E_{dis} = -7.0$  kJ/mol and  $E_{rep} = 4.0$  kJ/mol] with the molecule interacting at  $R = 14.68$  Å.

The above results show that the molecules with lesser distance have relatively strong interaction energy and vice versa, which also holds good with the laws of electrostatics. Further the interaction energy profile of each compound, in which the dispersion energies frame works dominates over the classical electrostatic energy frame works.

### 3.5. Molecular docking analysis

One of the most vigorous ways to tackle cancer is chemotherapy. In order to treat cancer cells different approaches are employed. Newer drugs are being developed with main focus on targeted therapy. One of the important approaches is the *in silico* molecular docking studies.

**Table 7.** Interaction energies (kJ/mol), R is the distance between molecular centroids (mean atomic position) in Å. Total energies, only reported for two benchmarked energy models, are the sum of the four energy components, scaled appropriately (see the scale factor table below) for compound **5e**.

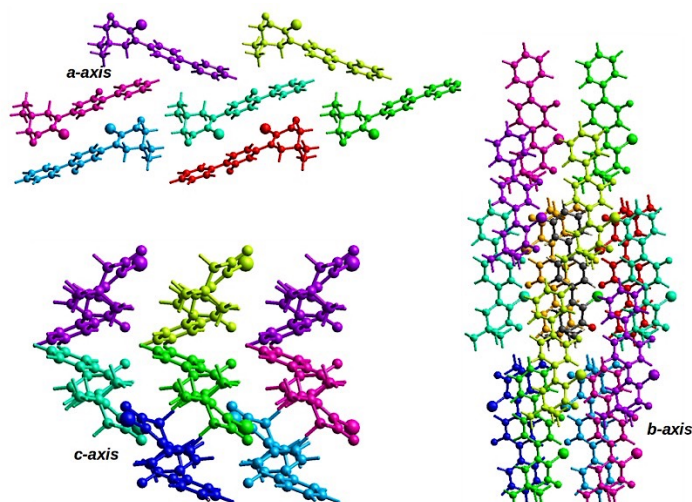
Color code	N	Symmetry	R	Electron density	$E_{ele}$	$E_{pol}$	$E_{dis}$	$E_{rep}$	$E_{tot}$
	1	-x, -y, -z	6.01	B3LYP/6-31G(d,p)	-8.7	-5.1	-34.7	27.6	-26.2
	1	-x, -y, -z	4.68	B3LYP/6-31G(d,p)	-18.7	-4.6	-59.4	34.0	-53.8
	2	x, -y+1/2, z+1/2	9.00	B3LYP/6-31G(d,p)	-4.4	-1.3	-32.9	14.6	-25.3
	2	x, y, z	14.21	B3LYP/6-31G(d,p)	0.3	-0.2	-7.8	3.3	-4.6
	2	x, y, z	6.49	B3LYP/6-31G(d,p)	-12.2	-2.7	-34.1	23.6	-30.1
	1	-x, -y, -z	12.80	B3LYP/6-31G(d,p)	-13.6	-4.5	-18.3	11.3	-26.6
	1	-x, -y, -z	13.75	B3LYP/6-31G(d,p)	-0.2	-0.4	-11.3	4.6	-7.6
	2	x, -y+1/2, z+1/2	10.17	B3LYP/6-31G(d,p)	-0.6	-0.4	-12.2	5.4	-8.3
	2	x, y, z	14.31	B3LYP/6-31G(d,p)	0.7	-0.1	-3.6	0.3	-2.3

Energy Model (30)	$K_{ele}$	$K_{pol}$	$K_{disp}$	$K_{rep}$
CE-HF ... HF/3-21G electron densities	1.019	0.651	0.901	0.811
CE-B3LYP ... B3LYP/6-31G(d,p) electron densities	1.057	0.740	0.871	0.618

**Table 8.** Interaction energies (kJ/mol), R is the distance between molecular centroids (mean atomic position) in Å. Total energies, only reported for two benchmarked energy models, are the sum of the four energy components, scaled appropriately (see the scale factor table below) for compound **5h**.

Color Code	N	Symmetry	R	Electron Density	$E_{ele}$	$E_{pol}$	$E_{dis}$	$E_{rep}$	$E_{tot}$
	2	x, y, z	11.08	B3LYP/6-31G(d,p)	-5.0	-2.2	-8.1	7.6	-9.3
	1	-x, -y, -z	14.68	B3LYP/6-31G(d,p)	0.7	-0.3	-7.0	4.0	-3.1
	2	x, y, z	6.75	B3LYP/6-31G(d,p)	-10.3	-3.0	-23.9	16.6	-23.7
	1	-x, -y, -z	7.74	B3LYP/6-31G(d,p)	-2.9	-1.4	-42.0	21.4	-27.5
	2	x, y, z	8.84	B3LYP/6-31G(d,p)	-3.7	-2.1	-27.2	13.0	-21.1
	1	-x, -y, -z	7.63	B3LYP/6-31G(d,p)	-0.3	-1.8	-33.0	17.9	-19.4
	1	-x, -y, -z	11.86	B3LYP/6-31G(d,p)	-1.7	-0.5	-15.4	11.7	-8.3
	1	-x, -y, -z	8.25	B3LYP/6-31G(d,p)	-9.7	-1.0	-21.2	19.7	-17.3
	1	-x, -y, -z	6.32	B3LYP/6-31G(d,p)	-7.6	-1.1	-30.9	17.7	-24.9
	1	-x, -y, -z	11.03	B3LYP/6-31G(d,p)	-12.4	-3.9	-15.9	7.9	-24.9

Energy Model (30)	$K_{ele}$	$K_{pol}$	$K_{disp}$	$K_{rep}$
CE-HF ... HF/3-21G electron densities	1.019	0.651	0.901	0.811
CE-B3LYP ... B3LYP/6-31G(d,p) electron densities	1.057	0.740	0.871	0.618

**Figure 6.** The color-coding pattern of molecules surrounding the original molecule in a cluster of molecule **5e** within the default radius of 3.8 Å, when it is viewed along crystallographic *a*, *b* and *c* axes. The color-coding scheme and their interaction energies in component form is given in [Table 7](#).

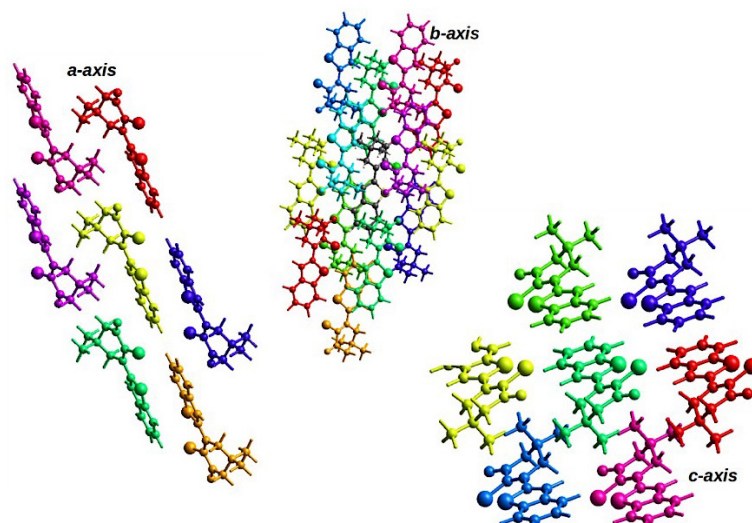


**Figure 7.** The color-coding pattern of molecules surrounding the original molecule in a cluster of molecule **5h** within the default radius of 3.8 Å, when it is viewed along crystallographic *a*, *b* and *c* axes. The color-coding scheme and their interaction energies in component form are given in [Table 8](#).

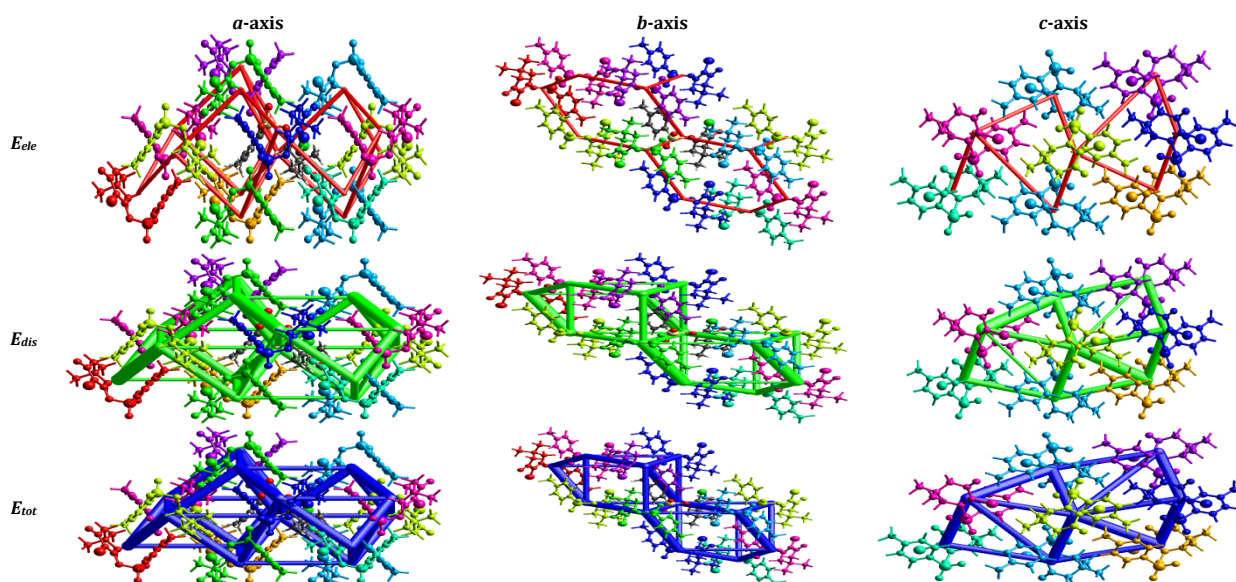


**Figure 8.** Energy frameworks corresponding to  $E_{ele}$ ,  $E_{dis}$ , and  $E_{tot}$  for molecule **3** when viewed along crystallographic *a*, *b* and *c* axes. The tube size maintained was 150 and the energy cut-off was 10 kJ/mol. The thickness of solid cylinders represents the relative strength of interaction.

In the present work, the molecules **5e** and **5h** were tested for its inhibitory action against h-ras (121p) by molecular docking studies. The free energy of binding for the compounds **5e** and **5h** with 121p was determined using PyRx 0.8 docking tool and nine different protein-ligand interactions were observed. [Tables 11](#) and [12](#) represent the list of binding energies for each interaction and their respective root mean square deviation (RMSD) values. The interactions of the protein with ligands **5e** and **5h** exhibiting least binding energies (-8.6 and -8.0 kcal/mol) were selected for further analysis. PyMOL representations of the docked ligands and proteins are represented in [Figure 11](#) and [12](#). The region of interaction between **5e** and the protein is represented in [Figure 11a](#), while [Figure 12a](#) represents the region of interaction between molecule **5h** and the protein. [Figures 11b](#), [11c](#), [12b](#), and [12c](#) represent the 3D plot of the regions of interaction between the ligands and the amino acids of the protein. A 2D plot was also generated which represents the amino acids involved in

hydrogen bonding and hydrophobic interactions with the ligand ([Figures 11d](#) and [12d](#)).

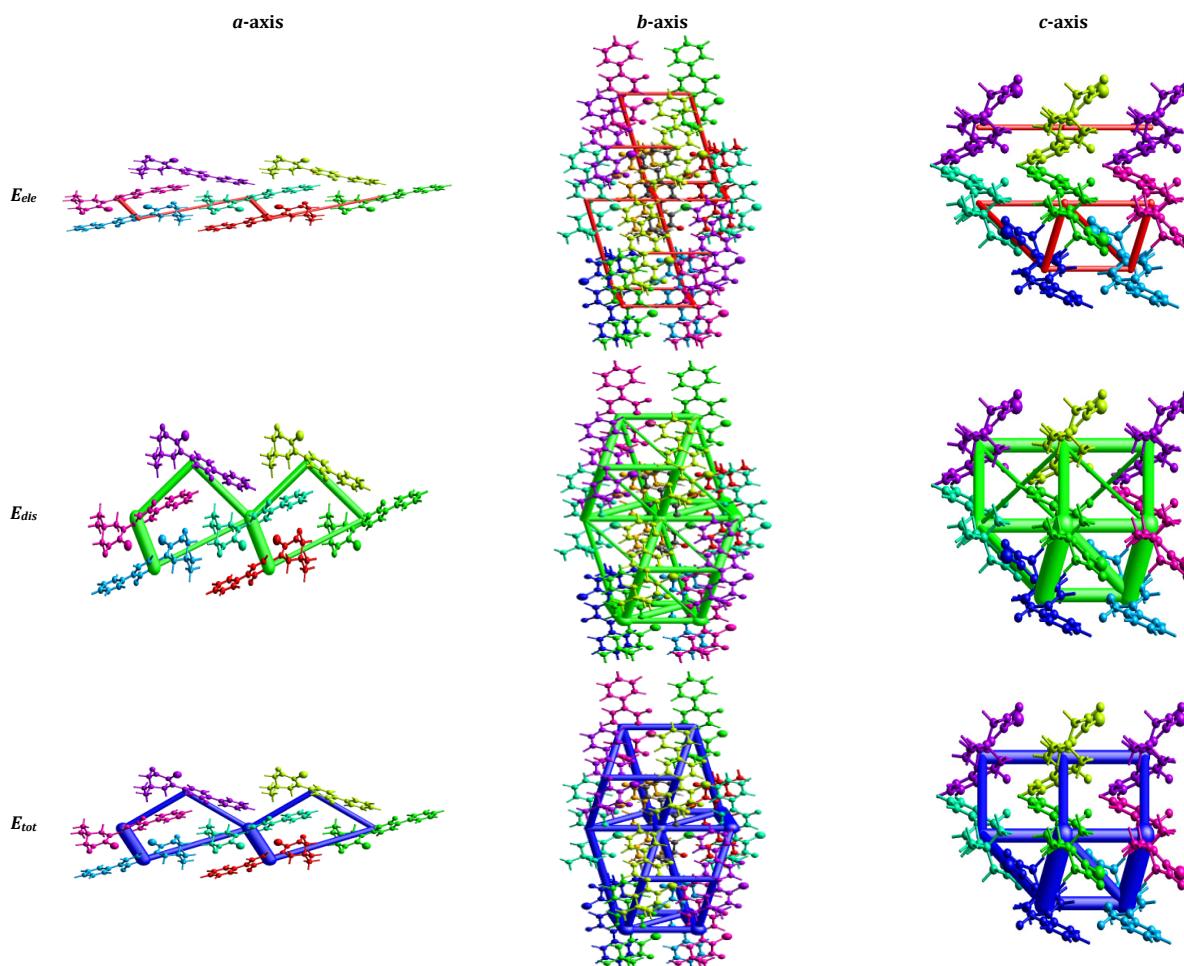
Ras genes belong to the class of oncogenes and the proteins they encode have been considered as potential targets for cancer therapy [31]. H-RAS genes encode H-ras protein, that is primarily a GTPase which converts GTP to GDP. This protein is involved in signal transduction from outside the cell to the nucleus to instruct the cell to grow and divide when bound to GTP. The enzyme is inactive or turned off when bound to GDP. Mutations in RAS genes result in H-ras proteins to remain in active state, thereby relaying the signal for cell division, leading to the growth of tumor. RAS mutations have been identified in more than 30% of the human tumors and 100% of the tumors in pancreatic cancer [32]. The docking results indicated molecule **5e** showing hydrogen bonding with the amino acid Asp33 with a bond distance of 3.15 Å, while Ser17, Glu31, Val29, Asp119, Phe28, Lys117, Gly15, Gly13, Tyr32 and Thr35 showed hydrophobic interactions ([Figure 11d](#)).

**Table 9.** The list of binding affinities and RMSD values of molecule **5e** interaction at different sites of H-ras.

Ligand	Binding affinity (kJ/mol)	RMSD (ub)	RMSD (lb)
121p_5e	-8.6	0	0
121p_5e	-8.6	2.188	1.281
121p_5e	-8.5	2.269	1.660
121p_5e	-8.5	8.053	2.809
121p_5e	-8.1	1.281	1.175
121p_5e	-7.7	7.620	2.584
121p_5e	-7.6	18.650	16.903
121p_5e	-7.0	8.028	3.079
121p_5e	-7.0	22.764	20.101

**Table 10.** The list of binding affinities and RMSD values of molecule **5h** interaction at different sites of H-ras.

Ligand	Binding affinity (kJ/mol)	RMSD (ub)	RMSD (lb)
121p_5h	-8.0	0	0
121p_5h	-8.0	2.944	1.505
121p_5h	-7.8	6.856	2.605
121p_5h	-7.0	7.848	4.680
121p_5h	-7.0	3.258	1.563
121p_5h	-6.9	1.729	1.353
121p_5h	-6.8	8.512	4.605
121p_5h	-6.7	5.854	3.658
121p_5h	-6.5	4.252	3.400

**Figure 9.** Energy frameworks corresponding to  $E_{ete}$ ,  $E_{dis}$ , and  $E_{tot}$  for molecule **5e** when viewed along crystallographic  $a$ ,  $b$  and  $c$  axes. The tube size maintained was 150 and the energy cut-off was 10 kJ/mol. The thickness of solid cylinders represents the relative strength of interaction.

However, the ligand **5h** showed only hydrophobic interactions with Glu31, Val29, Gly15, Ser17, Asp119, Asn116, Ala18, Phe28, Lys117 and Gly13 (Figure 10d). Janes *et al.* have reported the inhibitory action of ARS-1620 against KRAS [33]. Evidences show that GDP exhibits hydrogen bonding with various amino acids of H-ras such as Ser17, Gly13, Lys16, Gly15, Asp119, Ala146, Asn116, Val29, Asp30 and Ala18. Some of the

key amino acids found in the interaction of molecules **5e** and **5h** with H-ras are the same amino acids which are involved in hydrogen bonding with GDP. Hence, the molecules **5e** and **5h** could be potential inhibitors against H-ras. Further experimental studies would prove its ability to act as an inhibitor in anticancer therapies.

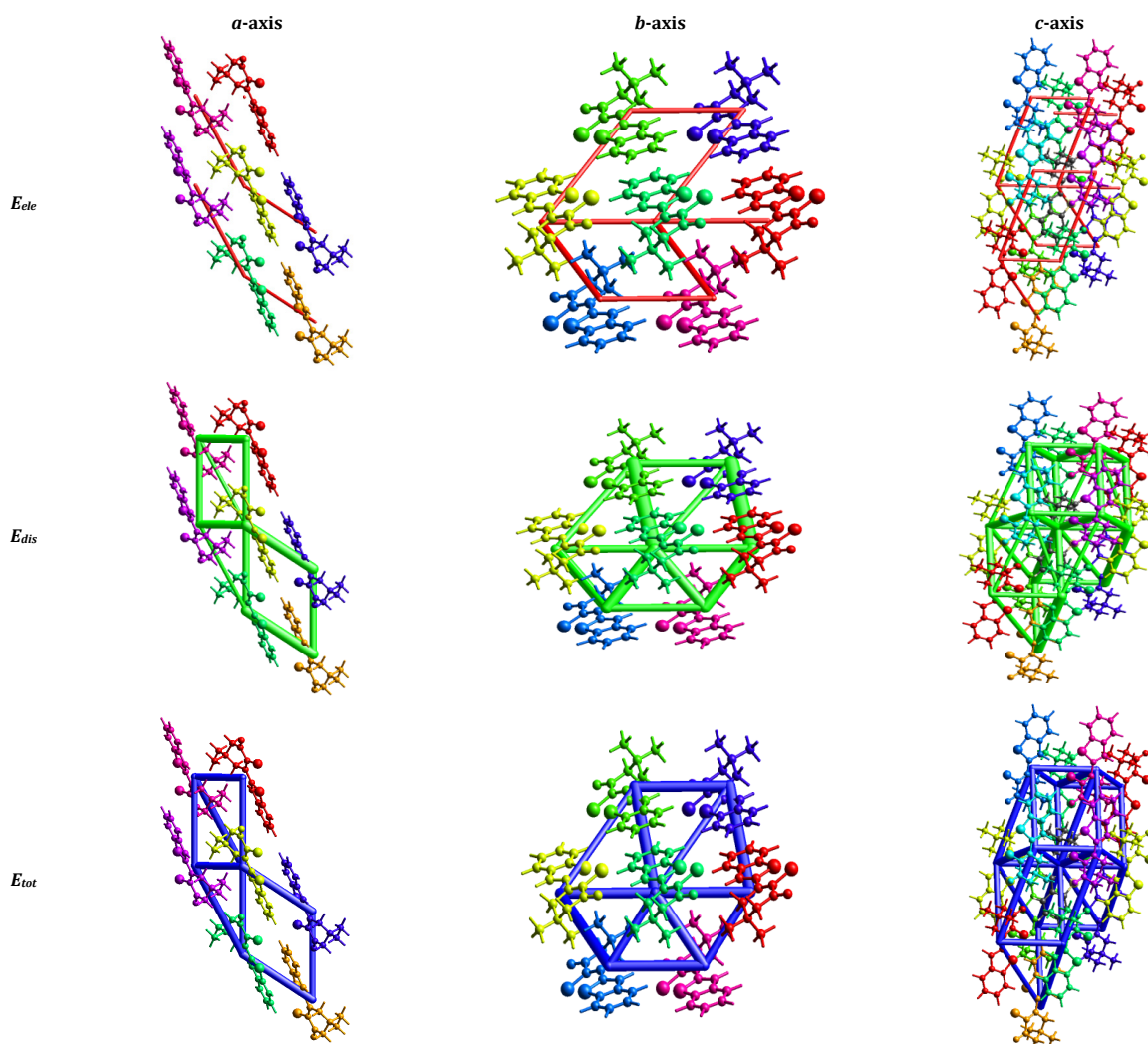


**Figure 10.** Energy frameworks corresponding to  $E_{elo}$ ,  $E_{dis}$ , and  $E_{tot}$  for molecule **5h** when viewed along crystallographic  $a$ ,  $b$  and  $c$  axes. The tube size maintained was 150 and the energy cut-off was 10 kJ/mol. The thickness of solid cylinders represents the relative strength of interaction.

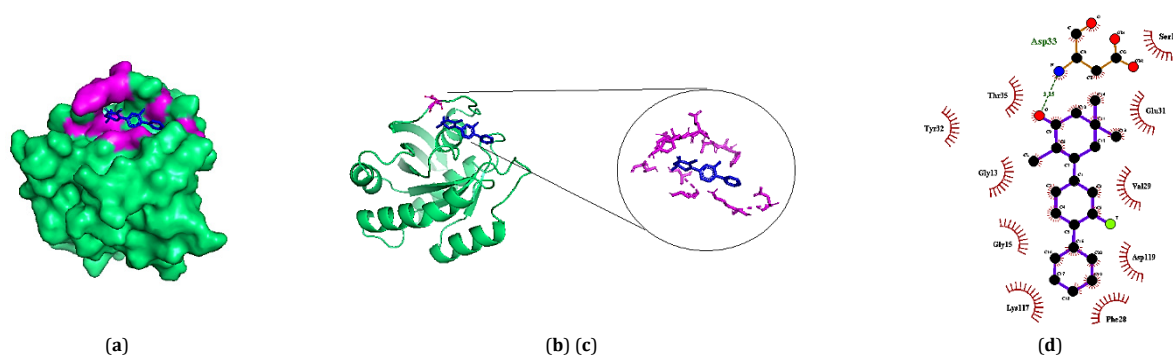


**Figure 11.** Molecular docking of molecule **5e** with H-ras. (a) Surface model representing the interacting site of H-ras (121p) with molecule **5e** (ligand). Blue color represents ligand and magenta color represents interacting amino acids of the protein. (b) Ribbon representation of the docked ligand with H-ras. (c) 3D representation of the ligand and the interacting amino acids. (d) 2D plot of interaction between ligand and amino acids of H-ras. Green line between the amino acids represents hydrogen bonding and other amino acids show hydrophobic interactions.

#### 4. Conclusion

In this article, we report an alternative route for the synthesis of 2-chloro-3-aryl-5,5-dimethylcyclohexenones. The successful regiospecific substitution of the vinylic tosylate group over the vinylic chloride group is highlighted. Single crystal XRD studies of three representative compounds are

discussed. The Hirshfeld surface studies confirmed the presence of intermolecular interactions of the type C-H $\cdots$ O, C-H $\cdots$ Cl and C-H $\cdots$ O in the compounds **3**, **5e** and **5h**, respectively. The two-dimensional fingerprint calculations showed that in the compounds **3** and **5e**, the H $\cdots$ O and H $\cdots$ H; whereas in molecule **5h** the H $\cdots$ H pairs of contacts have been served as major contributions towards crystal packing.

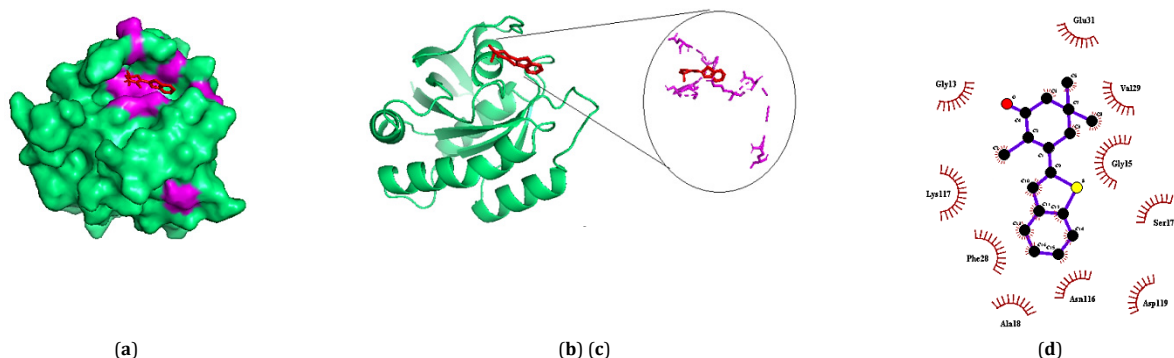


**Figure 12.** Molecular docking of molecule **5h** with H-ras. (a) Surface model representing the interacting site of H-ras (121p) with molecule **5h** (ligand). Red color represents the ligand and magenta color represents interacting amino acids of the protein. (b) Ribbon representation of the docked ligand with H-ras. (c) 3D representation of the ligand and the interacting amino acids. (d) 2D plot of interaction between ligand and amino acids of H-ras. Green line between the amino acids represents hydrogen bonding and other amino acids show hydrophobic interactions.

The three-dimensional interaction energy frame works were studied in all the compounds and the dispersion energy frame works dominated over classical energy frame works. Molecular docking of the products shows good scope for the utilization of the compounds as ligands in anti-neoplastic activity.

#### Acknowledgements

The authors thank the parent universities: (1) Bangalore University; (2) Bengaluru Central University for all facilities provided; (3) Arkalgud Satyanarayana Jeevan Chakravarthy is thankful to the Council of Scientific and Industrial Research (CSIR), Government of India, New Delhi, India, for providing financial support in the form of a Senior Research Fellowship - Direct, vide CSIR SRF - File no. 09/039(0119)/2018-EMR-1, dated April 16, 2018; (4) Grateful thanks is placed on record to the Sophisticated Analytical Instruments Facility (SAIF), Indian Institute of Technology, Madras, Chennai-600 036, Tamil Nadu, India, for XRD, data collection; (5) Mrs. Suchithra Bagepalli and Dr. Nagesh Babu, Department of Biochemistry, Maharani's Science College for Women, Bengaluru, for extending DST-FIST lab facilities and docking studies; (6) Mr. N. Rangapa Sreenatha, Department of Physics, Government Engineering College, Hassan-573 201, Karnataka, for reducing the crystal structure; (7) Dr. B. S. Bandodkar, Dr. M. A. Venkatesha and Avinash, Raju, Bangalore for all the help rendered. Taken in part from the PhD thesis of Arkalgud Satyanarayana Jeevan Chakravarthy, submitted to Bangalore University, Bangalore, India - August 2020.

#### Supporting information

CCDC-1875712, CCDC-1940404 and CCDC-1940405 contain the supplementary crystallographic data for this paper. These data can be obtained free of charge via <https://www.ccdc.cam.ac.uk/structures/>, or by e-mailing [data\\_request@ccdc.cam.ac.uk](mailto:data_request@ccdc.cam.ac.uk), or by contacting The Cambridge Crystallographic Data Centre, 12 Union Road, Cambridge CB2 1EZ, UK; fax: +44(0)1223-336033.

#### Disclosure statement

Conflict of interests: The authors declare that they have no conflict of interest.

Author contributions: All authors contributed equally to this work.

Ethical approval: All ethical guidelines have been adhered.

Sample availability: Samples of the compounds are available from the author.

#### Funding

Council of Scientific and Industrial Research, India  
<http://dx.doi.org/10.13039/501100001412>

#### ORCID

Arkalgud Satyanarayana Jeevan Chakravarthy

<http://orcid.org/0000-0003-3010-8402>

HariPrasad Suresh

<http://orcid.org/0000-0001-7157-1538>

#### References

- Li, Y.; Luo, Y.; Peng, L.; Li, Y.; Zhao, B.; Wang, W.; Lang, H.; Deng, Y.; Bai, R.; Lan, Y.; Yin, G. *Nature Commun.* **2020**, *11*, 417.
- Lee, H. W.; So, C. M.; Yuen, O. Y.; Wong, W. T.; Kwong, F. Y. *Org. Chem. Front.* **2020**, *7*, 926-932.
- Keaveney, S. T.; Kundu, G.; Schoenebeck, F. *Angew. Chem. Int. Ed. Engl.* **2018**, *130*, 12753-12757.
- Komeyama, K.; Tsunemitsu, R.; Michiyuki, T.; Yoshida, H.; Osaka, I. *Molecules* **2019**, *24*, 1458-1468.
- Chakravarthy, A. S. J.; Pavan, K. P.; Venkatesh, G. B.; HariPrasad, S. *Synthetic Commun.* **2020**, *50(6)*, 849-857.
- Chakravarthy, A. S. J.; Madhura, M. J.; Gayathri, V.; HariPrasad, S. *Tetrahedron Lett.* **2020**, *60(2)*, 151391.
- Chakravarthy, A. S. J.; Krishnamurthy, M. S.; Begum, N. S.; HariPrasad, S. *Mol. Cryst. Liq. Cryst.* **2019**, *682(1)*, 65-76.
- APEX2 Bruker, SAINT-Plus and SADABS, Bruker AXS Inc., Wisconsin, Madison, USA, 2004.
- Sheldrick, G. M. *Acta Cryst. C*, **2015**, *71*, 3-8.
- Spek, A. L. *Acta Cryst. C* **2015**, *71*, 9-18.
- Macrae, C. F.; Bruno, I. J.; Chisholm, J. A.; Edgington, P. R.; McCabe, P.; Pidcock, E.; Rodriguez-Monge, L.; Taylor, R.; van de Streek, J.; Wood, P. A. *J. Appl. Cryst.* **2008**, *41(2)*, 466-470.
- Sreenatha, N. R.; Lakshminarayana, B. N.; Ganesha, D. P.; Gnanendra, C. R. *Acta Cryst. E* **2018**, *74*, 1451-1454.
- Sreenatha, N. R.; Lakshminarayana, B. N.; Ganesha, D. P.; Vijayshankar, S.; Nagaraju, S. *X-Ray Struct. Anal. Online* **2018**, *34*, 24-25.
- Spackman, M. A.; Jayatilaka, D. *Cryst. Eng. Comm.* **2009**, *11*, 19-32.
- Spackman, M. A.; McKinnon, J. J.; Jayatilaka, D. *Cryst. Eng. Comm.* **2008**, *10(4)*, 377-388.
- McKinnon, J. J.; Jayatilaka, D.; Spackman, M. A. *Chem. Comm.* **2017**, 3814-3816.
- Turner, M. J.; McKinnon, J. J.; Wolff, S. K.; Grimwood, D. J.; Spackman, P. R.; Jayatilaka, D.; Spackman, M. A. *Crystal Explorer 17.5*. The University of Western Australia, 2017.
- Turner, M. J.; Grabowsky, S.; Jayatilaka, D.; Spackman, M. A. *J. Phys. Chem. Lett.* **2014**, *5*, 4249-4255.
- Sanner, M. F. *J. Mol. Graph. Mod.* **1999**, *17(1)*, 57-61.
- Wallace, A. C.; Laskowski, R. A.; Thornton, J. M. *Prot. Eng.* **1995**, *8(2)*, 127-134.
- McVeigh, M. S.; Kelleghan, A. V.; Yamano, M. M.; Knapp, R. R.; Garg, N. K. *Org. Lett.* **2020**, *22(11)*, 4500-4504.
- Geenen, S. R.; Schumann, T.; Mueller, T. J. *J. Org. Chem.* **2020**, *85(15)*, 9737-9750.
- Mpungose, P. P.; Vundla, Z. P.; Maguire, G. E. M.; Friedrich, H. B. *Molecules* **2018**, *23(7)*, 1676-1699.

- [24]. Boeyens, J. C. A. *J. Cryst. Mol. Struct.* **1978**, *8*, 317-320.
- [25]. Cremer, D. *Acta Cryst. B* **1984**, *40*, 498-500.
- [26]. Sreenatha, N. R.; Chakravarthy, A. S. J.; Suchithra, B.; Lakshminarayana, B. N.; Hariprasad, S.; Ganesha, D. P. *J. Mol. Struct.* **2020**, *1210*, 127979.
- [27]. Sreenatha, N. R.; Chakravarthy, A. S. J.; Lakshminarayana, B. N.; Hariprasad, S. *J. Mol. Struct.* **2021**, *1225*, 129116.
- [28]. Sreenatha, N. R.; Lakshminarayana, B. N.; Ganesha, D. P.; Gnanendra, C. R.; Nagaraju, S.; Madan, S. K. *Chem. Data Coll.* **2018**, *17-18*, 394-403.
- [29]. Sreenatha, N. R.; Lakshminarayana, B. N.; Madan, S. K.; Mahadeva, T. N. P.; Kiran, K. S.; Vijayshankar, D. S.; Byrappa, K. *Chem. Data Coll.* **2017**, *11-12*, 131-138.
- [30]. Mackenzie, C. F.; Spackman, P. R.; Jayatilaka, D.; Spackman, M. A. *IUCr* **2017**, *4(5)*, 575-587.
- [31]. Gysin, S. *Genes Cancer* **2011**, *2(3)*, 359-372.
- [32]. O'Bryan, J. P. *Pharmacol Res.* **2019**, *139*, 503-511.
- [33]. Janes, M. R.; Zhang, J.; Li, L. *Cell* **2018**, *172(3)*, 578-589.e17.



Copyright © 2020 by Authors. This work is published and licensed by Atlanta Publishing House LLC, Atlanta, GA, USA. The full terms of this license are available at <http://www.eurjchem.com/index.php/eurjchem/pages/view/terms> and incorporate the Creative Commons Attribution-Non Commercial (CC BY NC) (International, v4.0) License (<http://creativecommons.org/licenses/by-nc/4.0>). By accessing the work, you hereby accept the Terms. This is an open access article distributed under the terms and conditions of the CC BY NC License, which permits unrestricted non-commercial use, distribution, and reproduction in any medium, provided the original work is properly cited without any further permission from Atlanta Publishing House LLC (European Journal of Chemistry). No use, distribution or reproduction is permitted which does not comply with these terms. Permissions for commercial use of this work beyond the scope of the License (<http://www.eurjchem.com/index.php/eurjchem/pages/view/terms>) are administered by Atlanta Publishing House LLC (European Journal of Chemistry).